Carbon Nanotube Detection by Scanning Electron Microscopy

Tim Wortmann[1*] and Sergej Fatikow[1]

[1]Division Microrobotics and Control Engineering, University of Oldenburg, Germany

Abstract

This study describes an approach towards the detection of carbon nanotubes in scanning electron microscopic images. It is designed to work in a real-time environment for automated nanofabrication. Main difficulties are the high level of image noise and the occurrence of debris objects. A descriptor derived from the principle component analysis of the geometrical object distribution is found to be a very helpful indicator for object classification. It turns out to be largely invariant to alterations in imaging conditions. All methods described have been implemented and evaluated in large-scale experiments. The procedure has also been fully integrated into a distributed control architecture.

1 Introduction

Carbon nanotubes (CNTs) are one of the most promising materials in nanotechnologic applications. Their most interesting nanoelectric properties are the ballistic (scattering-free) and spin-conserving transport of electrons and their ability to show metallic as well as semiconductive behavior. Also, CNTs can handle a current density 1000 times higher than copper. This makes CNTs the perfect candidate for novel interconnects in the fabrication of integrated circuits [5]. Furthermore, nanoelectronic components such as the CNT field effect transistor have been built and show superior characteristics compared to silicon-based transistors [2][1]. Besides their nanoelectric properties, CNTs are also an auspicious material in nanomechanic applications.

Before these properties can be exploited in the large-scale production of nanodevices, reliable methods for automated handling and assembly of CNTs are needed. These differ significantly from the techniques used in conventional robotics because the behavior of nanoscale objects such as CNTs is considerably less predictable than that of macroscale objects. Visual feedback from scanning electron microscope images turned out to be the most important type of sensor feedback for this task. We present a CNT detection method than can be used for initial localization of CNTs from SEM images.

Section 2 will provide an overview of the current state of the art in automated CNT handling and also analyze the problem of visual CNT detection. The CNT detection method based on principle component analysis is described in section 3 and evaluated in multiple experiments in section 4.

2 Problem Analysis

Today, CNTs are commercially available and three different production methods are well-established: arc discharge, laser ablation and chemical vapor deposition (CVD). We focus on multi-walled CNTs grown by plasma enhanced CVD with a typical length of 10 - 20 µm and diameter of 150 - 350 nm but the results can be easily translated to other types of CNTs.

Electrothermal microgrippers have shown to be a useful tool for mechanical handling of individual CNTs. Latest approaches demonstrated pick-and-place handling of single CNTs following different goals including their electrical and mechanical characterization and the assembly of sensoric devices [7]. The utilization of visual feedback for the automation of CNT handling procedures focused on object tracking so far. Recent approaches include dedicated implementations of the active contours algorithm and 3D fitting of CAD models [3][9]. Nevertheless, these methods require manual initialization of object locations.

The main portion of noise in SEM images is caused by the secondary electron detector and is usually reduced using temporal averaging. This is why real-time processing of SEM images is always a tradeoff between image acquisition time and image quality. Figure 1 depicts this relationship showing multiple SEM images of an isolated CNT grown by CVD onto a silicon wafer. An acceptable acquisition time for full-frame CNT search is <1s. Another source of image degradation is grey level fluctuation which arises due to electrostatic charge and due to changes in the alignment of target, electron beam and detector.

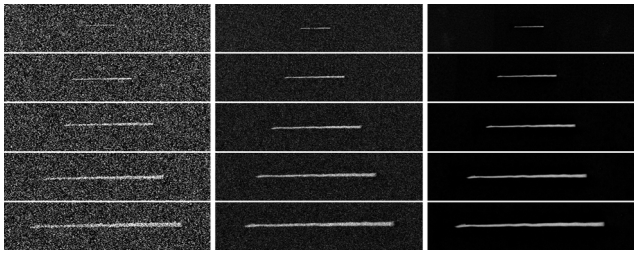

Figure 1: Sequence of SEM images of a multi-walled CNT with increasing level of magnification from 800x (top) up to 4000x (bottom) with a full-frame image acquisition time of 90ms/640ms/40.3s (left to right).

*This work was supported in part by the European Community: Project NANOHAND (IP 034274). Corresponding Author: wortmann@informatik.uni-oldenburg.de

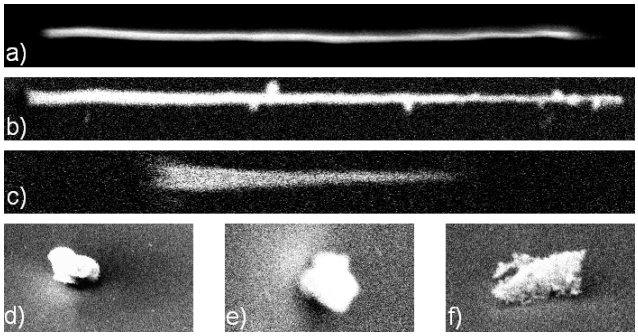

Figure 2: CNT rising out of the focus plane (a), material attached to CNT (b), conical shaped CNT (c), debris (d-f)

In the following, we describe the requirements to a CNT detection algorithm for the search of CNTs that are located at the surface of a silicon wafer. The algorithm must be fast enough for automation procedures and therefore handle a high level of image noise. It must detect CNTs at a wide range of different magnifications, different lengths and in any orientation. Depending on the fabrication process, multi-walled CNTs may be conically shaped. Evaporation of the electrothermal gripper may also lead to the deposition of material on the CNT surface. Although the SEM is considered to be an image sensor with high depth of field, a CNT may partly rise out of the focus plane. The algorithm must provide orientation and endpoints of CNTs and finally reliably reject any non-CNT particles that cannot be avoided if working under low cleanroom standards. Some of these requirements are illustrated in figure 2.

Combined with a scanning procedure, this algorithm will be able to provide a complete map of the wafer surface including CNTs and non-CNT objects. This information is intended to be used for the initialization of tracking algorithms that are needed for automated CNT handling. Additionally, it may be used as an error recovery sequence.

Because of its robustness to noise, normalized cross-correlation (NCC) is frequently used in SEM vision applications. High correlation coefficients between a sample pattern and the image to be analyzed indicate a hit of the object in demand. It has to be noted that NCC is very sensitive to object size, image scale, rotation and variations in object shape. Therefore, it does not meet the requirements stated above and is not appropriate to the problem.

3 Proposed Method

In the previous section we discussed that depending on the imaging conditions, CNT fabrication process and manipulation history only few assumption can be made regarding the appearance of CNTs in SEM images. One assumption that holds in practically every case is the idea that the outline of a CNT can be approximated by a straight line. Since other objects or structures found on the substrate tend to arrange and shape in a chaotic or round way this property will be exploited for CNT detection. Three commonly used methods for straight line detection were considered.

The active contour algorithm can be reformulated for straight line detection [6]. It uses an inner contour energy depending on line straightness and an outer contour energy derived from the image gradient perpendicular to the contour. This method is not suitable for our problem since the image gradient is highly sensitive to noise and because thick lines result in double hits.

Another algorithm for straight line detection is the Hough transform. Each point in Hough space corresponds to a line object in the input image, defined by angle and offset. Peaks in Hough space are used to identify dominant line objects. A disadvantage of the Hough transform is its high computational cost.

The principle component analysis (PCA) is a tool well-known in multivariate statistics. In the context of pattern recognition it is mainly used for dimension reduction of the input feature space. However, applied to the geometrical distribution of an object, it may also be utilized for straight line detection [4]. An ideal straight line in two-dimensional space has a principle component that can be calculated from the eigenvectors and eigenvalues of its scatter matrix. The scatter matrix $\mathbf{S}$ is an estimate of the covariance matrix that is derived from the geometrical distribution of n line points $\mathbf{X} = [\mathbf{x}_1, \mathbf{x}_2, \ldots, \mathbf{x}_n]$:

$$\mathbf{S} = \sum_{i=1}^{n} (\mathbf{x}_i - \overline{\mathbf{x}}) (\mathbf{x}_i - \overline{\mathbf{x}})' \quad \textit{where} \quad \overline{\mathbf{x}} = \frac{1}{n} \sum_{j=1}^{n} \mathbf{x}_j \ .$$

Since $\mathbf{S}$ is positive semidefinite, we can compute two non negative eigenvalues $\lambda_{1,2}$ and corresponding eigenvectors $\mathbf{v}_{1,2}$. The absolute values of $\lambda_{1,2}$ depend on scale and line length. A normalized score indicating line straightness is obtained from

$$\mathrm{PC_E} = \frac{2 \cdot \lambda_1}{\lambda_1 + \lambda_2} - 1 \ .$$

We will now explain how PCA can be applied to achieve robust CNT detection.

Noise Reduction SEM image noise is assumed to be Poisson-distributed due to the small number of secondary electrons measured by the detector. The median filter is expected to provide good results in this case because it is capable of edge preservation and shot noise removal. In our application, median filtering is critical because it removes thin lines from the image, e.g. CNTs that we are looking for. Therefore, we use simple Gaussian low-pass filtering in addition to temporal averaging. Gaussian filtering also removes high-frequency image detail which is irrelevant to our problem.

Image Segmentation It has to be noted that the CNT detection presented here does not rely on a perfect object segmentation from the background. Locally adaptive thresholding techniques turned out to be sensitive to slight variations in substrate brightness. Consequently we choose a global thresholding strategy. By experiment, we compare three methods which derive a threshold value from the image grey level histogram [8]: Gaussian mixture modeling (GMM), within-class variance minimization and class-entropy maximization. All methods successfully separate CNT and debris objects from the substrate at

a wide range of brightness. However, in image scenes showing only the substrate, the GMM and variance-based approaches fail to grade the whole image as background. For this reason we select class-entropy maximization for image segmentation.

Object Retrieval Individual objects are identified in the binary segmented image as 8-connected pixel-clouds. Object holes are filled afterwards. As this problem has a unique solution and is solved by any naive approach in acceptable time the actual implementation is irrelevant. We used an exterior contour retrieval algorithm with additional region filling. For m objects we receive m object point sets $\mathbf{X}^1 \dots \mathbf{X}^m$.

Principle Component Analysis PCA is applied to every point set $\mathbf{X}^1 \dots \mathbf{X}^m$ individually and we obtain the principle component energy scores $\mathrm{PC}_\mathrm{E}^1 \dots \mathrm{PC}_\mathrm{E}^m$. A score of $\mathrm{PC}_\mathrm{E} = 1$ corresponds to an ideal straight line whereas if the score is $\mathrm{PC}_\mathrm{E} = 0$ no dominant direction is found. This would be the case if the object is a circular disc. Single point objects are excluded because the corresponding scatter matrix $\mathbf{S}$ is singular. The eigenvectors $\mathbf{v}_{1,2}$ of each object form a rotation matrix which is used to transform each set of object points $\mathbf{X}^1 \dots \mathbf{X}^m$ into the its own PCA space. We receive $\hat{\mathbf{X}}^1 \dots \hat{\mathbf{X}}^m$.

Endpoint Retrieval From each set of transformed object points $\hat{\mathbf{X}} = [\hat{\mathbf{x}}_1, \hat{\mathbf{x}}_2, \dots, \hat{\mathbf{x}}_n]$ we calculate two peak positions

$$\hat{\mathbf{p}}_1 = \left[\min_{i \in 1 \dots n} \left\{ \hat{\mathbf{x}}_i \cdot \binom{1}{0} \right\}, 0 \right]^T$$

$$\hat{\mathbf{p}}_2 = \left[\max_{i \in 1 \dots n} \left\{ \hat{\mathbf{x}}_i \cdot \binom{1}{0} \right\}, 0 \right]^T .$$

Transforming $\hat{\mathbf{p}}_{1,2}$ back to image coordinates, we obtain an estimate of the CNT endpoints $\mathbf{p}_{1,2}$. Figure 3 depicts the working principle of PCA applied to the geometrical distribution of a CNT image.

Object Classification The principle component energy based score PC_E is a meaningful indicator for CNT objects. However, if an object is formed by only a few points the result becomes arbitrary. For this reason we need to check the object size for plausibility. We define a rough measure of object size using the relative projection area n, an appropriate scaling factor k_{P_A} and magnification scale M: $\mathrm{P}_A = k_{P_A} \cdot \sqrt{n}/M$. The decision boundary is learned automatically by training a Support Vector Machine (SVM) classifier [10] based on PC_E and P_A.

4 Experimental Results

The algorithm has been implemented to prove its capabilities in real-world experiments. Main studies have been carried out using a LEO 1450 by Zeiss. For comparison additional tests have been made using a Quanta 600 by FEI. Both SEMs are equipped with additional image acquisition hardware by Point Electronic. The silicon wafer is movable by piezoelectric actuators.

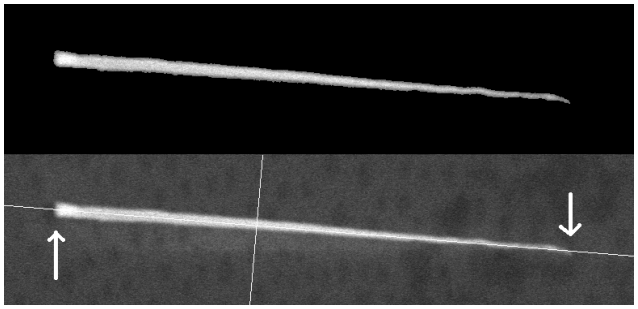

Figure 3: Masked CNT image after segmentation (upper), detected principal and secondary component of CNT's geometrical distribution (lower). The two arrows point at $\mathbf{p}_{1,2}$.

Initially, we investigated the influence of imaging conditions on the outcome of the segmentation method. Both SEMs come with an automated brightness and contrast adjustment which aims at best usage of the dynamic range. We studied the effect of variations in brightness and found the segmentation procedure largely insensitive as long as the object contrast remains sufficient.

In section 2, we outlined the importance of feature invariance to rotation, scaling and translation. These properties have been evaluated using a representative CNT object. For this purpose a sequence of 60 images was taken. The orientation was changed using electron beam rotation. Magnification was varied from 800x to 4000x. As expected, the features are almost invariant to translation and scale within the limits of numerical calculations and noise ($\sigma^2(\mathrm{PC}_\mathrm{E}) = 4.79 \cdot 10^{-8}$, $\sigma^2(\mathrm{P}_\mathrm{A}) = 6.12 \cdot 10^{-4}$). Changing the object orientation relative to the scanning direction effects contrast and shadows introducing a higher level of variation which is still uncritical for object classification ($\sigma^2(\mathrm{PC}_\mathrm{E}) = 5.61 \cdot 10^{-7}$, $\sigma^2(\mathrm{P}_\mathrm{A}) = 6.70 \cdot 10^{-3}$).

A collection of 300 image scenes was used to generate statistics of possible object shapes. Some of them can be seen from figures 5 and 6. 1177 objects were identified manually which included 432 CNTs. Small parts broken from CNTs were marked as debris as they are useless for our purposes. Figure 4 shows the histogram of PC_E for CNT and debris objects. All CNTs obtain high values of PC_E. Conical shaped CNTs and those with material attached to them were already included here. Small debris objects come in arbitrary

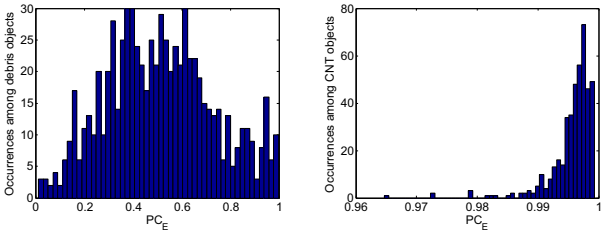

Figure 4: Statistics of principle component energy score PC_E for debris and CNT objects. Values of CNT objects cluster close to $\mathrm{PC}_\mathrm{E} = 1$ while debris objects fill the whole range.

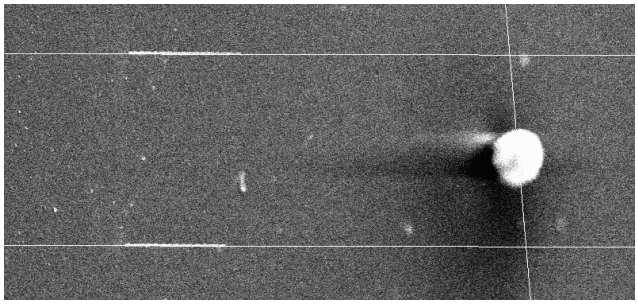

Figure 5: Image scene assessed by the proposed algorithm. Principle component directions are indicated. The two CNTs obtain a PC_E of 0.9988 and 0.9987 - the debris object 0.1457 respectively.

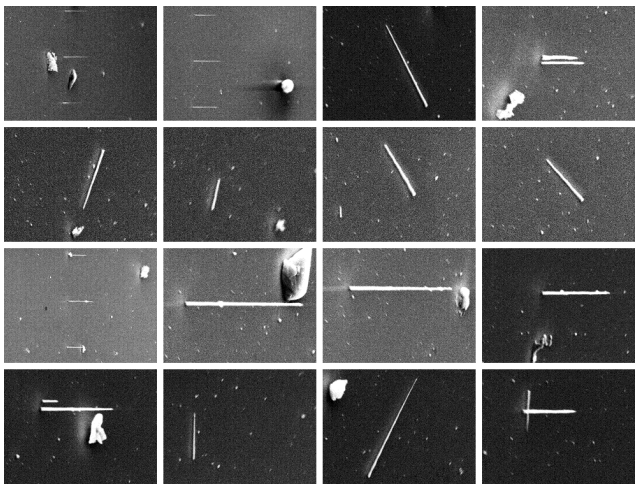

Figure 6: Selection of image scenes collected during the experiments at magnifications ranging from 800x to 4000x. A total number of 1177 objects were identified in the complete set and used for training: 432 CNTs and 745 debris objects.

shape which occasionally results in high values of PC_E. Instead of manually choosing thresholds for PC_E and P_A, we train a linear SVM on our statistics.

The algorithm has been fully integrated into a pre-existing distributed control architecture for automated nanohandling of CNTs. It sends commands to and recieves results from the computer vision application via a CORBA interface. All actuators as well as the SEM control are available via the common interface. This allows us to test the detection algorithm in its dedicated application environment without any manual interaction. An automation script was written which scans the wafer surface through the SEMs field of view. The vision application detects and classifies objects from the images. Only if CNTs are detected, the object endpoint coordinates are transmitted to the controller. The controller uses its knowledge of the wafer position to translate the image coordinates to world coordinates.

For testing, the wafer used in training was exchanged in order to provide a new set of objects. The scan was performed along multiple straight lines which are 500 µm in length. Throughout multiple test sequences no CNT was detected incorrectly (false positive). However a few CNTs were ignored which were attached to or occluded by large debris objects. Also, the algorithm is not able to separate CNTs crossing each other (figure 6, lower right scene). This is not contrary to the aim of this work which is the detection of isolated CNTs on the substrate that can be revisited for automated nanohandling.

The accuracy of the CNT endpoint coordinates could not be evaluated due to the lack of a measurement method for comparison. By manually inspecting the collected data we find most endpoints placed correctly. Some misplacements occur if the CNT tip is out of focus. In that case the detected tip position is shifted towards the CNT center.

This algorithm shows a data-dependent processing time which was below the image acquisition time for all real-world experiments. It has to be noted that the magnifications mentioned in this document are calibrated for a 17" display with a resolution of 1280 x 1024 pixel.

5 Conclusion

The proposed method provides a powerful means of CNT detection using the SEM. Combined with an object tracking procedure it enables automated handling of individual CNTs with a wide range of possible applications. Reliability and real-time capability have been proven in large-scale experiments under a wide range of imaging conditions. The results are also applicable to other types of CNTs including single-walled CNTs.

References

[1] P. Avouris, J. Appenzeller, R. Martel, and S. Wind. Carbon nanotube electronics. *Proc. of the IEEE*, 91 (11):1772 – 1784, 2003.

[2] W. Hoenlein, F. Kreupl, G. Duesberg, A. Graham, M. Liebau, R. Seidel, and E. Unger. Carbon nanotube applications in microelectronics. *IEEE Transactions on Components and Packaging Technologies*, 27 (4):629 – 634, 2004.

[3] B. Kratochvil, L. Dong, and B. Nelson. Real-time rigid-body visual tracking in a scanning electron microscope. In *Proc. of the 7th IEEE Conf. on Nanotechnology (IEEE-NANO2007), Hong Kong, China*, August 2007.

[4] Y.-S. Lee, H.-S. Koo, and C.-S. Jeong. A straight line detection using principal component analysis. *Pattern Recogn. Lett.*, 27(14):1744–1754, 2006.

[5] P. Patel-Predd. Carbon-nanotube wiring gets real. *IEEE Spectrum*, 45 (4):14, 2008.

[6] R. Rodrigo, W. Shi, and J. Samarabandu. Energy based line detection. In *Canadian Conference on Electrical and Computer Engineering*, 2006.

[7] O. Sardan, V. Eichhorn, D. Petersen, S. Fatikow, O. Sigmund, and P. Bøggild. Rapid prototyping of nanotube-based devices using topology optimized microgrippers. *Nanotechnology*, 2008.

[8] M. Sezgin and B. Sankur. Survey over image thresholding techniques and quantitative performance evaluation. *J. of Electronic Imaging*, 13 (1):146–165, 2004.

[9] T. Sievers and S. Fatikow. Real-time object tracking for the robot-based nanohandling in a scanning electron microscope. *Journal of Micromechatronics - Special Issue on Micro/Nanohandling*, 3(3-4):267–284(18), 2006.

[10] I. Steinwart and A. Christmann. *Support Vector Machines*. Information Science and Statistics. Springer, 2008.